Aust. J. Phys., 1991, **44**, 277–91

The Development of Electron Momentum Spectroscopy*

Erich Weigold

Electronic Structure of Materials Centre, Flinders University of South Australia, G.P.O. Box 2100, Adelaide, S.A. 5001, Australia.

Abstract

The study of the valence electronic structure of atoms and molecules by (e, 2e) spectroscopy, or EMS as it is now known, began in the early 1970s with a series of measurements at Flinders University. The first measurements were on argon, and they showed the importance of correlation effects in the inner valence 3s shell. The first molecular experiments were on methane, and they showed the sensitivity of the momentum distributions to details of the orbital wavefunctions. Until recently all EMS measurements were made on ground state targets with random orientations. We have, however, now made successful EMS measurements on excited states and oriented targets. Sodium atoms in the $3^2S_{1/2}(F=2)$ ground state are optically pumped by right-handed circularly polarised light to the excited $3^2P_{3/2}(F'=3, m_{F'}=3)$ state. Thus the excited atoms are all in the $|\ell=1, m_\ell=1\rangle$ state. These measurements are discussed in some detail.

1. Historical Introduction

It is a great pleasure to contribute this paper to the collection in honour of Ian Ellery McCarthy. He played a pioneering and guiding role in the development of electron momentum spectroscopy (EMS), or (e, 2e) spectroscopy. He continues to play that role. It began in 1960 when he, Baker and Porter (Baker *et al.* 1960) speculated about the possibility of making momentum distribution measurements in atoms with suitable probes. During the 1960s he and I discussed the possibility of doing experiments in atomic physics analogous to the nuclear physics experiments designed to reveal structure information. These discussions started in the early 1960s at the University of Adelaide, and were later pursued in more detail in the USA. We were particularly interested in seeing whether the (e, 2e) reaction could be developed in atomic physics as an analogue to the (p, 2p) reaction in nuclear physics. Little did we realise then that it would develop into a much more successful probe of atomic and molecular structure than the (p, 2p) reaction in determining nuclear structure.

Following the early speculations of Baker *et al.* (1960), Smirnov and Neudatchin (1966) pointed out the potential advantages of the (e, 2e) reaction for investigating the electronic structure of atoms, molecules, and solids. A detailed plane-wave impulse approximation (PWIA) formalism for atoms, molecules and thin films was given by Neudatchin *et al.* (1968). Glassgold

* Dedicated to Professor Ian McCarthy on the occasion of his sixtieth birthday.

0004-9506/91/020277$05.00

and Ialongo (1968) gave a plane-wave Born approximation formalism for the (e, 2e) reaction.

In the meantime Ian McCarthy was busy convincing me that it was nice to be poor in Australia and that I should come to Flinders University. Immediately on my arrival in September of 1970, I started designing an (e, 2e) coincidence spectrometer. The construction of the spectrometer and the associated electronics and vacuum system was not completed until 1972. At that stage Stephen Hood, Peter Teubner and I started to test and tune the apparatus. By late 1972 we had some fascinating results on the valence shell of argon. At about the same time Camilloni *et al.* (1972) reported the first measurement of an orbital momentum distribution, namely the 1s core orbital of solid carbon, which they obtained with a 90 eV uncertainty in the binding energy in a 9000 eV experiment. The energy resolution was far too poor to resolve any structure in the valence region.

Our measurements were the first on free atoms, the first to resolve structure in the valence region and to measure valence orbital momentum distributions.

2. Theoretical Background

In (e, 2e) spectroscopy the momenta $\mathbf{p}_0, \mathbf{p}_A$ and $\mathbf{p}_B$ of the three electrons are observed, with the outgoing ones A and B detected in fast coincidence. The quantities of primary interest are related to the observed momenta and corresponding kinetic energies E_0, E_A and E_B. They are the recoil momentum $\mathbf{p}$ of the target

$$\mathbf{p} = \mathbf{p}_0 - \mathbf{p}_A - \mathbf{p}_B , \tag{1}$$

and the electron separation energy ϵ_f, which is the energy eigenvalue of a state f of the residual ion,

$$\epsilon_f = E_0 - E_A - E_B . \tag{2}$$

The total energy E is given by

$$E = E_A + E_B = E_0 - \epsilon_f . \tag{3}$$

As in photoelectron spectroscopy, EMS observes the energy spectrum ϵ_f of the residual ion. Its unique value lies in its role as a probe for the distribution of the momentum $\mathbf{q}$ of target electrons for ion states f. At high enough energies and suitable kinematic conditions, momentum is transferred to the outgoing electrons only by a collision with a moving target electron, in which case

$$\mathbf{q} = -\mathbf{p} . \tag{4}$$

In quantum mechanics this momentum probe is represented by the electron impact ionisation amplitude from ground state 0,

$$T = \langle \mathbf{p}_A \mathbf{p}_B f \mid t_S(E) \mid 0 \mathbf{p}_0 \rangle , \tag{5}$$

where $t_S(E)$ is the amplitude for collision of two electrons with total kinetic energy E and total spin S. The absolute square of this amplitude gives the coincidence count rate for ionisation. It factorises as follows:

$$T = \langle \mathbf{k}' \mid t_S(k'^2) \mid \mathbf{k} \rangle \langle f \mid a(\mathbf{q}) \mid 0 \rangle, \tag{6}$$

where the first factor is the half-off-shell Coulomb t-matrix element for the e–e collision and the second factor is the target–ion overlap amplitude resulting from the annihilation of an electron of momentum $\mathbf{q}$ in the target ground state 0. In equation (6),

$$\mathbf{k}' = \tfrac{1}{2}(\mathbf{p}_A - \mathbf{p}_B), \quad \mathbf{k} = \tfrac{1}{2}(\mathbf{p}_0 - \mathbf{q}). \tag{7}$$

The e–e collision factor in (6) is approximately constant for both noncoplanar symmetric and coplanar Bethe ridge kinematics. These are the EMS conditions. Equation (5) describes the PWIA, which is the basic approximation of EMS. Its validity is expected to improve with increasing energy until structure determination becomes independent of energy. For randomly oriented targets the (e, 2e) differential cross section in the PWIA is equal to the spherically-averaged square of the electronic overlap multiplied by a number which is essentially constant for an experiment at a particular value of the total energy E. This means that it is independent of ϵ_f and q. The information about the target and ion structure is contained in the electronic overlap. In the one-electron model of the target,

$$\langle f \mid a(\mathbf{q}) \mid 0 \rangle = \psi_f(\mathbf{q}), \tag{8}$$

where $\psi_f(\mathbf{q})$ is the orbital for the one-hole state f. In this model EMS observes the orbital momentum distribution.

To understand the electronic overlap we consider the configuration interaction (CI) expansion of target and ion states in determinants (configurations) formed by occupying target Hartree–Fock orbitals by electrons in such a way that each configuration has the symmetry of the state. The configuration with all the lowest orbitals occupied is the Hartree–Fock configuration. The representation we will use to describe ion correlations is not the CI representation, but one in which the orthonormal basis states $\mid j \rangle$ are linear combinations of configurations formed by annihilating one electron in a target eigenstate. The target eigenstate may of course be expressed in the CI representation. The ion representation is the weak-coupling representation. The basis states $\mid j \rangle$ are weak-coupling states. Note that the weak-coupling states are identical to the CI configurations if the target is uncorrelated, i.e. represented by the Hartree–Fock configuration (the target Hartree–Fock approximation).

The weak-coupling expansion of the target–ion overlap is

$$\langle f \mid a(\mathbf{q}) \mid 0 \rangle = \sum_j \langle f \mid j \rangle \langle j \mid a(\mathbf{q}) \mid 0 \rangle. \tag{9}$$

Clearly, $\langle j \mid a(\mathbf{q}) \mid 0 \rangle$ is zero if $\mid j \rangle$ is not a one-hole state $\mid i \rangle$ formed by annihilating an electron from the orbital i in the target ground state.

The weak-coupling approximation has turned out to be usually valid. Here the weak-coupling expansion of the ion state $|f\rangle$ contains only a single one-hole state $|i\rangle$,

$$\langle f|a(\mathbf{q})|0\rangle = \langle f|i\rangle\langle i|a(\mathbf{q})|0\rangle. \tag{10}$$

The weak-coupling approximation is a generalisation of the target Hartree–Fock approximation (THFA) to the situation where target correlations are not negligible.

The PWIA differential cross section in this approximation is proportional to the square of the one-hole overlap $\langle i|a(\mathbf{q})|0\rangle$, which is the momentum-space orbital for the target. We define the experimental orbital $\psi_i(\mathbf{q})$ by

$$\psi_i(\mathbf{q}) \equiv \langle i|a(\mathbf{q})|0\rangle. \tag{11}$$

The differential cross section is proportional also to the spectroscopic factor

$$S_f^{(i)} = |\langle f|i\rangle|^2, \tag{12}$$

which is the probability of the one-hole configuration $|i\rangle$ contributing to the weak-coupling expansion of the ion state $|f\rangle$.

The form used for the differential cross section in the PWIA is

$$\frac{d^5\sigma}{d\hat{\mathbf{p}}_A d\hat{\mathbf{p}}_B dE_A} = (2\pi)^4 \frac{p_A p_B}{p_0} f_{ee} S_f^{(i)} (4\pi)^{-1} \int d\hat{\mathbf{q}}\, |\psi_i(\mathbf{q})|^2, \tag{13}$$

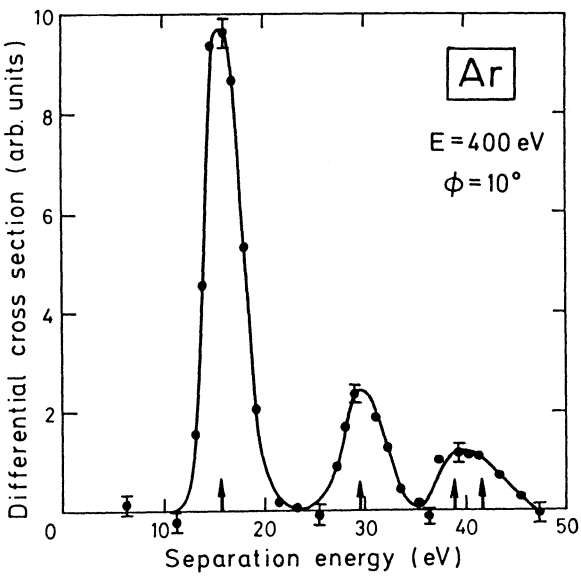

Fig. 1. The differential cross section at $\phi = 10°$ for the 400 eV noncoplanar symmetric (e, 2e) experiment on argon (Weigold *et al.* 1973*a*). The arrows indicate known energy levels of Ar^+.

where the *ee* collision factor f_{ee} is the absolute square of the half-off-shell Coulomb *t*-matrix element (equation 6), summed and averaged over final and initial electron spin states. Under EMS conditions it is essentially independent of q up to about 2 a.u. at $E = 1000$ eV. For oriented targets, or if magnetic degeneracies are resolved, as for instance in laser excitation, the spherical average in (13) need no longer be taken. We will treat this case later.

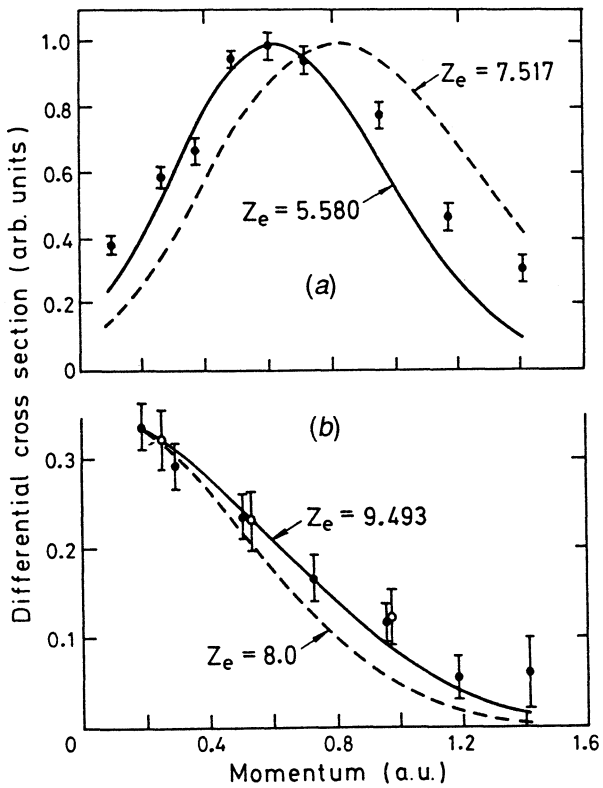

Fig. 2. The momentum distributions for (*a*) the 3p and (*b*) 3s electrons in argon. In (*b*) the solid circles are for the 29·3 eV transition and the open circles for the peak at 40 eV after multiplication by a factor of 1·3. The solid and dashed curves are the momentum distributions for screened hydrogenic wavefunctions with the indicated values of the effective charge (from Weigold *et al.* 1973*a*).

3. The First EMS Measurements for Atoms and Molecules

Fig. 1 shows the distribution of electron separation energies for argon observed at $\phi = 10°$ for a total energy of 400 eV in the first EMS measurement on atoms (Weigold *et al.* 1973*a*). The evidence of final state correlations is evidenced by the fact that there are more ion states than the two we expect from holes in the valence 3p and 3s orbitals, whose Hartree–Fock energies are 16 and 35·4 eV respectively. The structure around 40 eV puzzled us greatly. At that time there was no evidence for such structure in photo-electron spectra (PES) or x-ray electron spectra (ESCA). Its angular correlation was the same as that for the peak at 29·3 eV, which was the expected $3s^{-1}$ peak according to PES. The 29·3 eV peak was found to contain only 0·58±0·04 of the strength

of the 3s transition, in excellent agreement with the present accepted value of 0·55±0·01 (McCarthy and Weigold 1988). This unexpected splitting of the 3s hole resulted in a significant delay in publication of the results, since we wanted to be certain of its interpretation. This work also showed that measured momentum distributions provide sensitive tests of the orbital wavefunctions. Fig. 2 shows the momentum distributions obtained by Weigold *et al.* (1973*a*) compared with two simple wavefunctions.

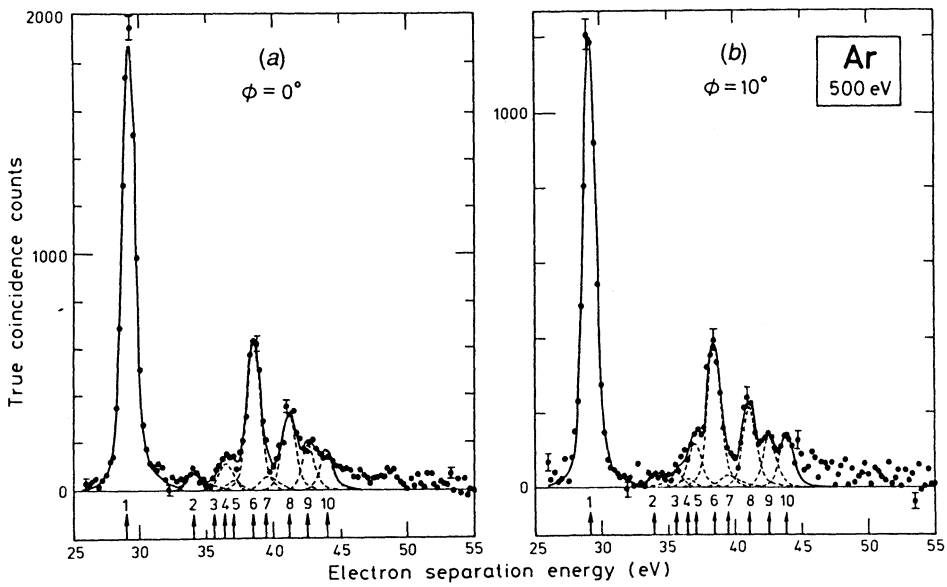

Fig. 3. The 500 eV noncoplanar symmetric EMS separation energy spectra at (*a*) $\phi = 0°$ ($p \sim 0{\cdot}2$ a.u.) and (*b*) $\phi = 10°$ ($p \sim 0{\cdot}6$ a.u.) (McCarthy *et al.* 1989). The curves show fitted spectra using the known energy resolution. The assignments for the peaks are discussed by McCarthy *et al.* Peaks 1, 4, 6, 8, 9 and the high energy structure belong to the $^2S^e$ manifold, 2 to the $^2D^e$ manifold, 3 and 5 to the $^2P^0$ manifold, and peak 7 to either the $^2P^0$ or $^2D^e$ manifold.

Fig. 3 shows for comparison with Fig. 1 some recent separation energy spectra over the range 29–55 eV (McCarthy *et al.* 1989). All of the structure, except peaks 2, 3, 5 and 7, belongs to the ^2S (i.e. 3s) manifold. Peak 2 arises from *d*-wave correlations in the argon ground state, and peaks 3 and 5 belong to the ^2P manifold. Peak 7 probably contains both ^2D as well as ^2P contributions. Fig. 4*a* shows the angular correlation obtained by them at 1500 eV for the 3p ground state transition, and Fig. 4*b* the angular correlation for the 3s manifold (crosses) and the 29·3 eV transition (filled circles), compared with the calculated cross sections using Hartree–Fock 3p and 3s wavefunctions. Both PWIA and DWIA calculations are shown. These approximations were largely developed by I.E. McCarthy (e.g. Hood *et al.* 1973*a*; McCarthy and Weigold 1976). McCarthy *et al.* measured the spectroscopic factors for the $3p^{-1}$ ground state of the ion to be 0·95±0·02 and that for the $3s^{-1}$ state at 29·3 eV to be 0·55±0·01. The DWIA–HF calculation completely describes the measured

momentum distributions, the PWIA giving good shapes out to momenta of about 1–1·5 a.u. The data are normalised to the DWIA calculation at one point, namely at $\phi = 10°$ for the 3p ground state transition. Many-body calculations are generally inadequate in describing the correlation effects in the 3s manifold (McCarthy and Weigold 1988), and the argon atom still provides a challenge to many-body theories.

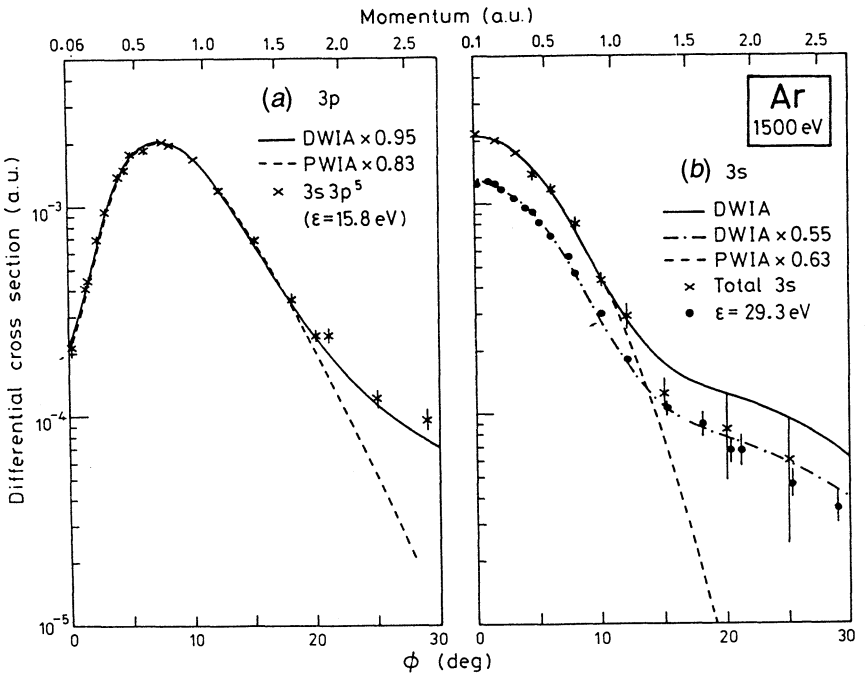

Fig. 4. The 1500 eV noncoplanar symmetic momentum profiles for (*a*) the Ar ground state transition ($\epsilon = 15·8$ eV), and (*b*) the first excited state ($\epsilon = 29·3$ eV), and the total $^2S^e$ manifold compared with the DWIA and PWIA cross sections using HF 3p and 3s wavefunctions. All the data have been normalised by fitting the measured ground state transition to 0·95 times the 3p DWIA cross section, the spectroscopic factor for the ground state transition being 0·95 (McCarthy *et al.* 1989).

The first molecule to be studied by the (e, 2e) technique was methane (Hood *et al.* 1973*b*), although its actual publication followed our first work on molecular hydrogen (Weigold *et al.* 1973*b*). In methane, as in argon, we found significant structure in the inner valence region in addition to the two dominant transitions belonging to the $1t_2$ and $2a_1$ valence orbitals. This structure was assigned to the $2a_1$ orbital on the basis of the measured momentum distributions.

Fig. 5 shows the momentum distribution obtained by Hood *et al.* for the outer valence $1t_2$ orbital of CH_4 compared with momentum distributions given by a number of simple molecular orbital wavefunctions. These first measurements on molecules demonstrated the sensitivity of the momentum distributions to details of molecular wavefunctions. This sensitivity has been used to great effect to study molecular structure (e.g. McCarthy and Weigold 1988).

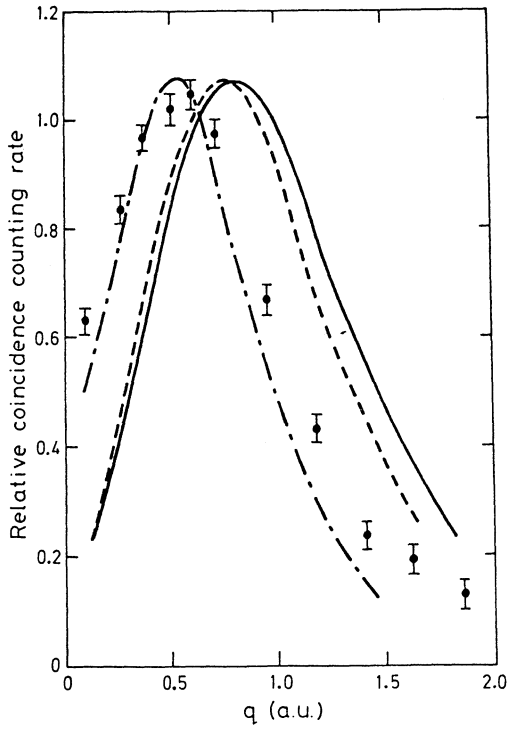

Fig. 5. Momentum profile for the $1t_2$ orbital of methane observed in a 400 eV noncoplanar symmetric ionisation experiment (Hood *et al.* 1973*b*). PWIA curves are calculated with simple molecular orbitals. Full curve: Pitzer (1967), dashed curve: Palke and Lipscombe (1966), dash–dot curve: SCF (Froese-Fischer 1972).

4. Electron Momentum Spectroscopy of Laser Excited Atoms

We recently carried out the first (e,2e) measurements on a target in an excited state as well as the first on an oriented target (Zheng *et al.* 1990). Excited target atoms can be prepared in well defined states by optically pumping atoms with a tuneable laser. Further, by using polarised laser light it is possible to excite specific magnetic substates. This offers the possibility of measuring momentum distributions for excited targets as well as for atoms in aligned or oriented states.

In the measurements of Zheng *et al.* sodium atoms are optically pumped by right-hand circularly polarised laser light tuned to the $3^2S_{1/2}(F=2) \leftrightarrow 3^2P_{3/2}(F'=3)$ transition. The excited pumped atoms are in the $m_{F'} = 3$ state, or in terms of orbital momentum in the $m_\ell = +1$ state. The coordinate frame is chosen so that the electron momentum density of the excited state was probed in the q_x direction with q_z and q_y being fixed and essentially zero.

The experimental arrangement is shown in Fig. 6. A detailed description of the multi-parameter coincidence spectrometer and the associated circuitry is given elsewhere (Weigold 1990, McCarthy and Weigold 1990, Weigold *et al.* 1991). The sodium oven (Fig. 7) is mounted out-of-the-plane of Fig. 6 and produces a well collimated sodium beam perpendicular to and intersecting the horizontal laser beam and vertical electron beam, thus defining the interaction region. The sodium source consists of a vertical cylindrical stainless steel oven with a horizontal 32 mm long and 0·8 mm diameter effusive nozzle mounted close to the top of the oven. The oven and nozzle are separately heated with their temperature being typically 400° and 500°C respectively.

In order to obtain the highest fraction of the population in the $3^2P_{3/2}(F'=3)$ excited state, the Doppler broadening of the sodium beam has to be limited to about 20 MHz. This means that the sodium beam has to be well collimated with a maximum divergence of about 1°. The sodium beam is trapped by a refrigerated finger to keep the electron spectrometers and vacuum clean.

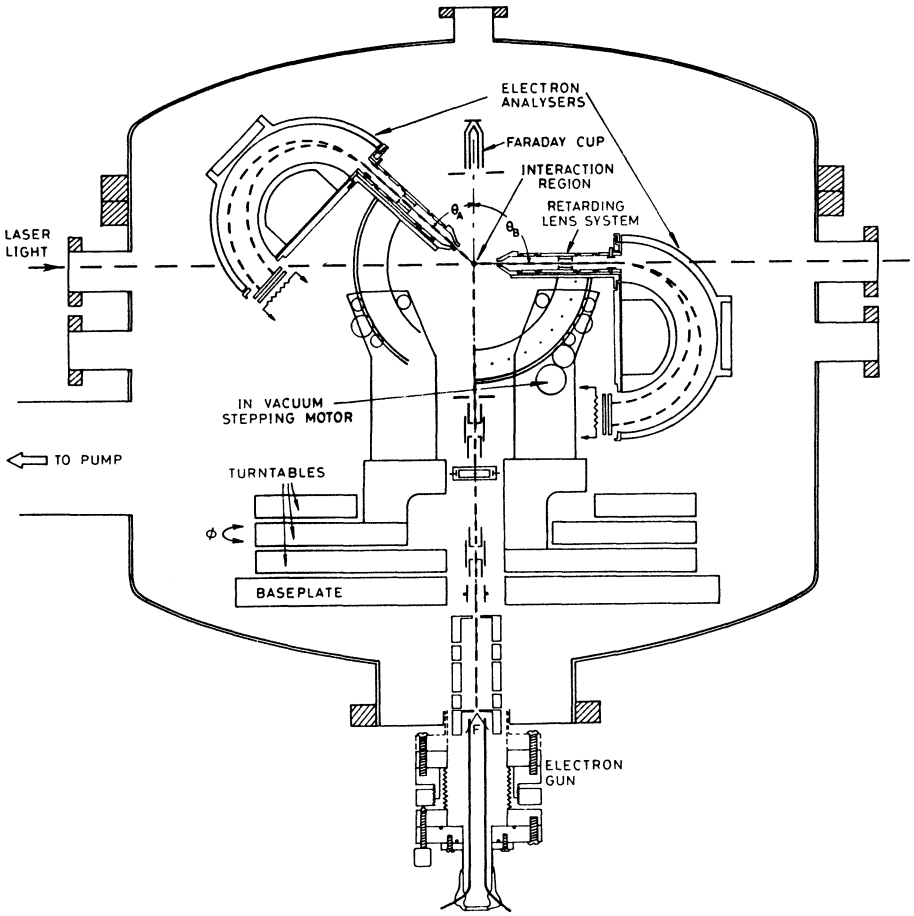

Fig. 6. Schematic view of the multi-parameter (e, 2e) coincidence spectrometer. The electron beam, laser beam, and sodium beam intersect at right angles. The sodium oven (not shown) is mounted perpendicular to the plane of the diagram. In the measurements $\theta_A = \theta_B = 45°$ and $\phi = \phi_A - \phi_B - \pi$. The hemispherical energy analysers are preceded by a five element retarding and focusing lens. The position sensitive detector at the exit aperture of the analyser determines the arrival time and the energy of each detected electron.

The optical arrangement used is shown in Fig. 8. An argon ion laser pumps a tunable CW ring dye laser whose light is then right-handed circularly polarised using a linear polariser and quarter-wave plate. A split photodiode is used to keep the laser tuned to the $3^2S_{1/2}(F=2) \rightarrow 3^2P_{3/2}(F'=3)$ transition for atoms in the narrow sodium beam. The fluorescence from the decay of the $3^2P_{3/2}(F'=3)$ state back to the $3^2S_{1/2}(F=2)$ ground state is imaged with a simple lens onto the split photodiode. Due to the small but finite divergence of the

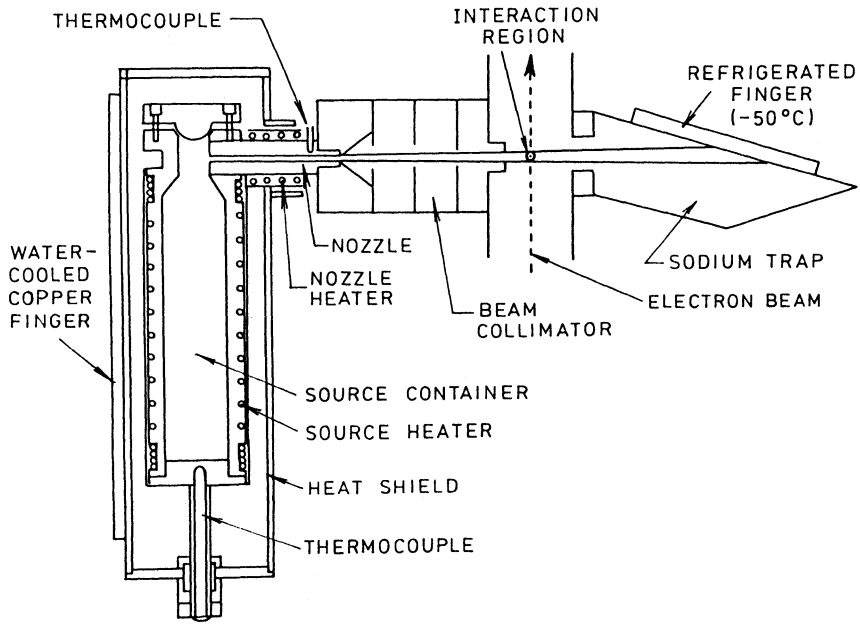

Fig. 7. Sodium oven and beam source.

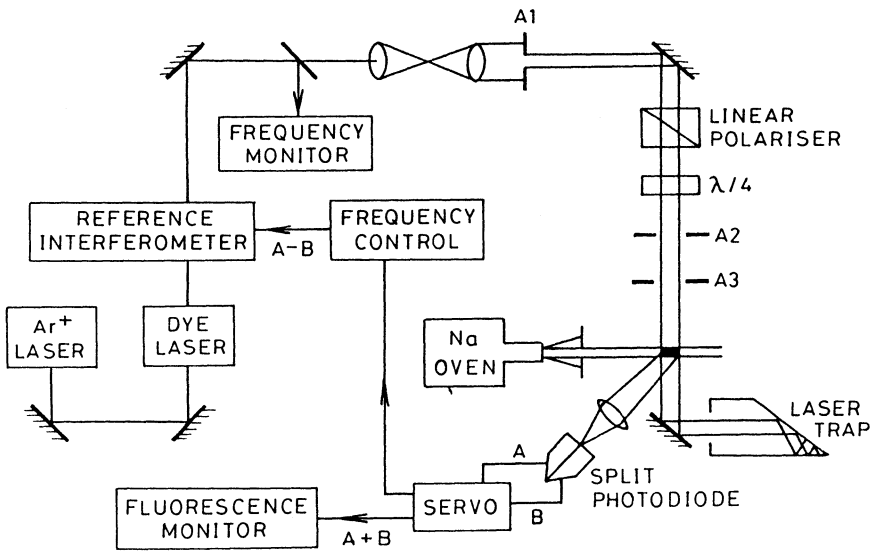

Fig. 8. The arrangement of the optical system for laser excitation of sodium atoms. For details see text.

sodium beam, the atoms in that part of the atomic beam moving towards the laser beam absorb light at a slightly lower frequency than those travelling away from the laser beam. Thus the brightest portion of the fluorescence spot is seen to move if the frequency of the laser drifts slightly. When the spot moves, one half of the split photodiode receives more signal than the other,

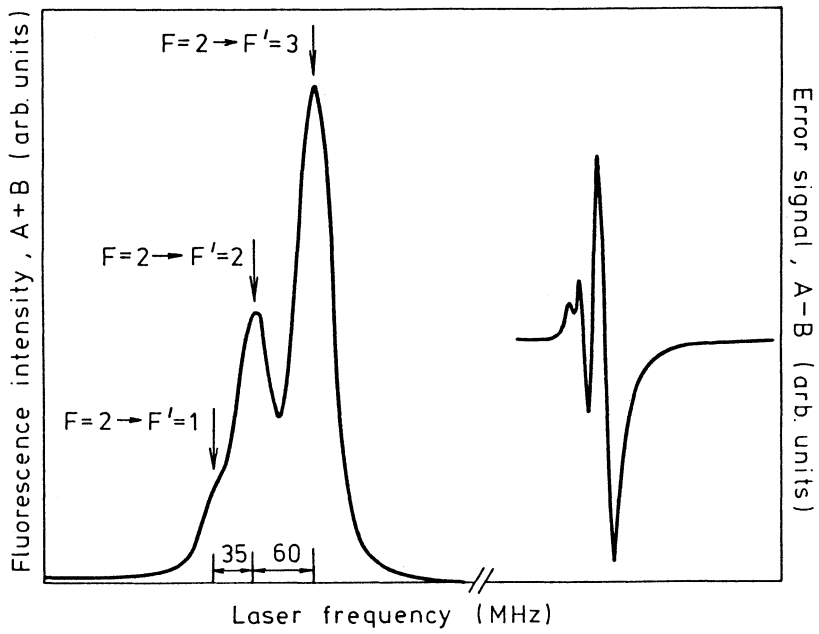

Fig. 9. Frequency lock characteristics of the split photodiode outputs A and B.

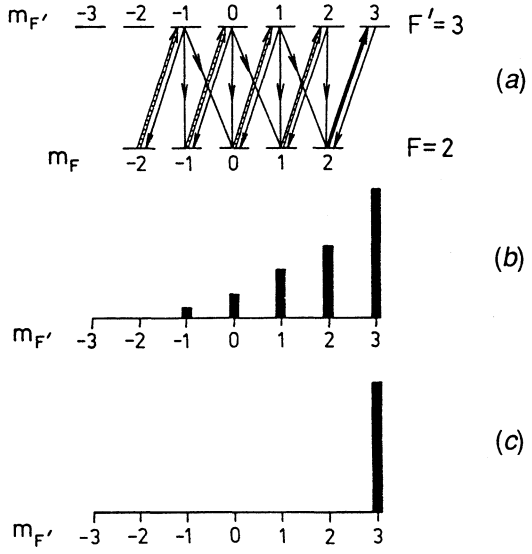

Fig. 10. Optical pumping of sodium D_2 line with σ^+ light: (*a*) scheme of cyclic pumping; (*b*) the relative populations in the $F' = 3$ excited state at the initial stage; and (*c*) the stationary condition.

and vice versa. The difference between the two photodiode signals, A–B, is then used as an error signal in a feedback loop which controls the frequency of the dye laser. This locking scheme is most useful for compensating slow drifts in laster frequency, since fast changes are quite well controlled by the laser's own active stabilisation. The sum signal of the split photodiode, A+B, provides information on the intensity of the laser and the density of the

atomic beam. The plot of fluorescence intensity and error signal versus laser frequency is shown in Fig. 9. The plot is obtained with the laser power very much reduced to eliminate power broadening.

A beam expander, consisting of two lenses and an aperture A1 is inserted in the laser beam, so that only a narrow section of the beam is used, creating a semi-constant radiation intensity across the pump region. In this way uncertainty due to the gaussian profile of the pump laser is avoided. In the stationary condition this pumping with σ^+ light produces a population of the $F = 2, m_F = 2$ ground state with about 12% of the beam in the $F' = 3, m_{F'} = 3$ excited state (see Fig. 10). This means that in the excited state there is no population in the $m_\ell = 0$ (i.e. $3p_z$) orbital, all being in the $m_\ell = +1$ state, corresponding to 50% in both the $3p_x$ and $3p_y$ orbital. The momentum densities for the three degenerate orbitals are shown schematically in Fig. 11, the $3p_z$ orbital being of course unoccupied.

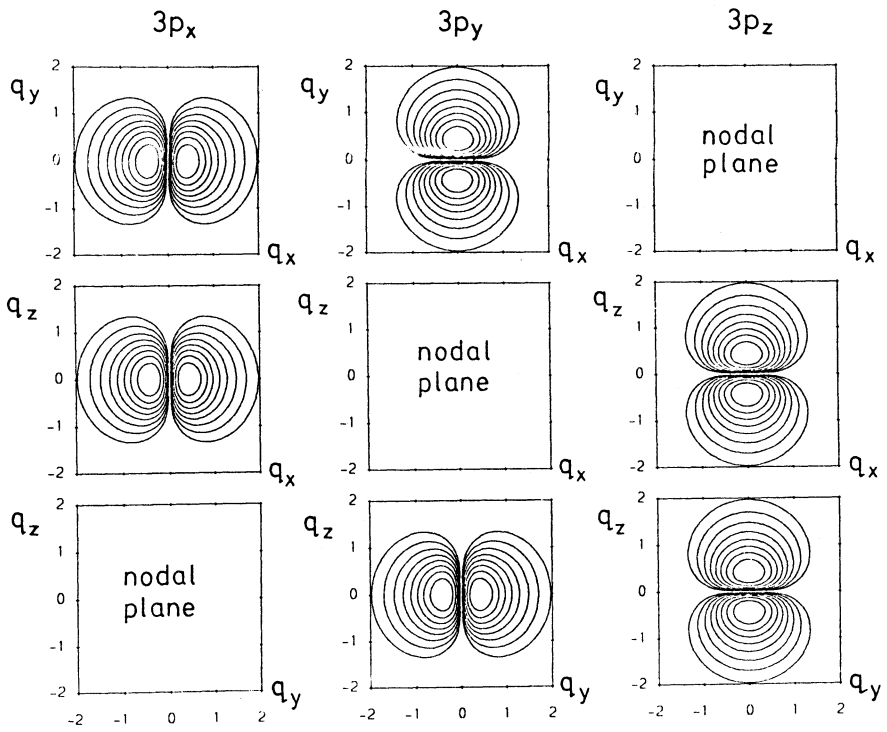

Fig. 11. Schematic momentum density contour maps of the three degenerate 3p orbitals. The measurement probes the momentum density of the $3p_y$ orbitals along the q_x axis, the $3p_z$ orbital being occupied.

The axis of quantisation z has been with chosen as the direction of propagation of the circularly polarised pumping beam, with the atomic sodium beam incident in the x direction and the electron beam incident in the y direction. This is shown schematically in Fig. 12, which also shows schematically the $3p_z$ and $3p_y$ distribution of the charge cloud of the sodium in the $3p(m_\ell{=}{+}1)$ excited

state. The scattering plane is the zy plane and both outgoing electrons make a polar angle of 45° with respect to the incident (y) direction. The out-of-plane azimuthal angle θ of electron B is varied to probe the different momentum components of the target. Thus the experiment measures the (e, 2e) triple differential cross section as a function of the x component of momentum, q_x. For the symmetric noncoplanar kinematics employed, $E_A = E_B = 400$ eV and $\theta_A = \theta_B = 45°$, the z and y components of momenta are fixed and essentially zero for small binding energies. Due to the finite angular and hence momentum resolution of the spectrometer, the average values of q_y and q_z are not quite zero, being of the order of 0·06 a.u.

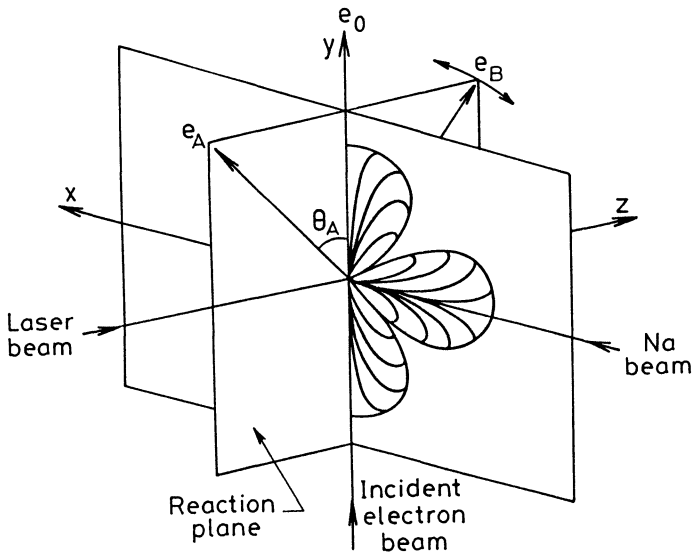

Fig. 12. Schematic diagram of the experimental arrangement and the electron charge and momentum densities of the excited 3p(m_ℓ=1) sodium atoms. The momentum is probed along the x direction with $q_y \sim q_z \sim 0$.

Fig. 13 shows the separation energy spectra obtained at $\phi = 2·5°$ for (*a*) no laser light and (*b*) with the laser on. Ionisation from atoms in the excited $^2P_{3/2}$ state can be seen quite clearly. The momentum distributions obtained for the 3s ground state transition and for the 3p(m_ℓ=1) excited state are shown in Figs 14*a* and 14*b*, respectively, compared with calculated momentum distributions given by the Hartree–Fock 3s and 3p(m_ℓ=+1) wavefunctions. The finite angular (i.e. momentum) resolution has been included in the calculations. The main effect of the finite angular resolution is to fill in the $3p_x$ momentum distribution at momenta close to zero. The momentum distribution for the excited state peaks at very small momenta (~ 0·2 a.u.) because of the diffuse nature of the 3p orbital in coordinate space. Also shown in the figure for comparison is the momentum distribution expected for the $m_\ell = 0$ substate of the 3p state. That for the unoriented $3p_{(0,\pm1)}$ state is similar to that for the $m_\ell = 1$ substate, but is in significantly poorer agreement with the data due to the inclusion of the $m_\ell = 0$ component. The momentum distribution for the $m_\ell = 0$ (i.e. $3p_z$) state is of course zero along the q_z axis ($q_y = q_z = 0$), since

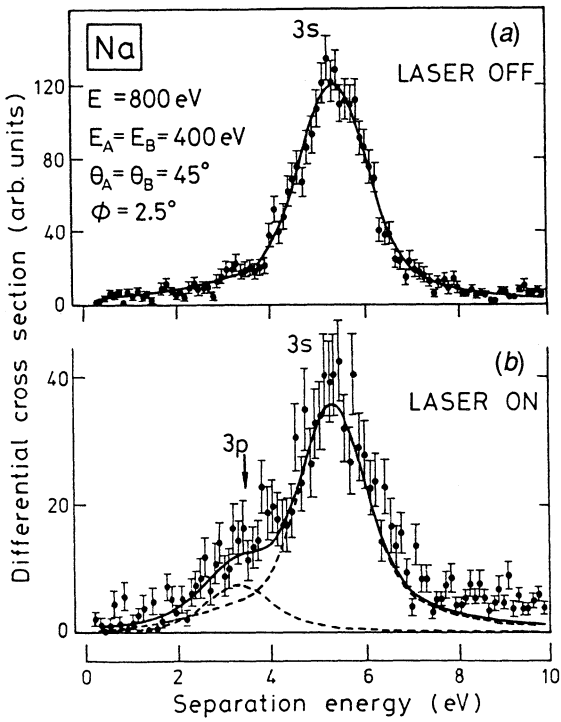

Fig. 13. The 800 eV noncoplanar symmetric separation energy spectra at $\phi = 2{\cdot}5°$ for sodium with (*a*) laser off and (*b*) laser on.

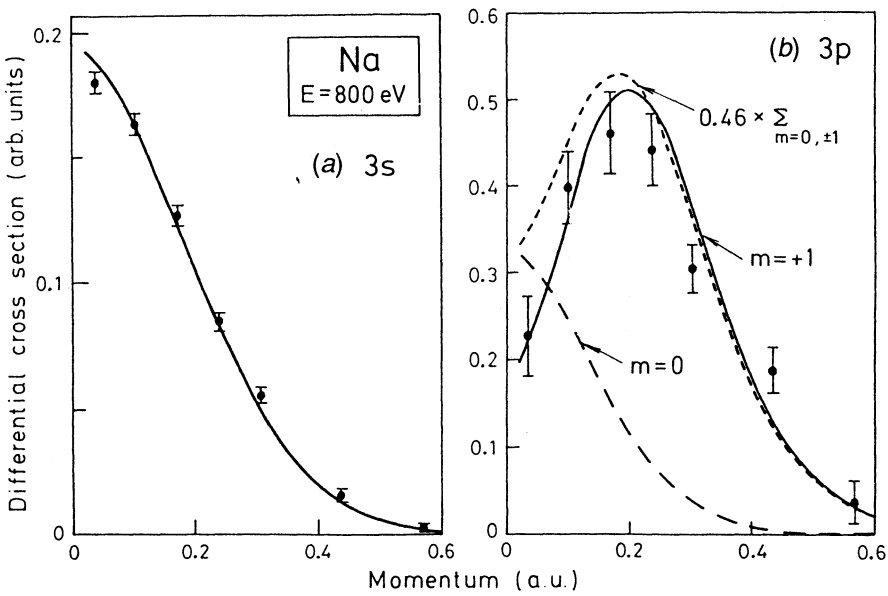

Fig. 14. The measured and calculated momentum distributions for (*a*) the 3s ground state and (*b*) the 3p excited state of Na (Zheng *et al.* 1990). The solid curve in (*a*) is the HF 3s momentum profile and in (*b*) the 3p(m_ℓ=+1) profile, the long dashed curve that expected for the $m_\ell = 0$ component. The PWIA calculations have the experimental angular resolution folded in. The momentum is probed along the q_x axis.

the $3p_z$ (dumbbell) orbital is perpendicular to the nodal $x-y$ plane, the node being at the origin. However, due to the finite momentum resolution, there is a finite probability of seeing some $m_\ell = 0$ contribution if there were any atoms in this excited magnetic substate, this probability decreasing as one moves away from the origin along the q_z (or for that matter the q_y) direction. This explains the 'anomalous' shape of the calculated $m_\ell = 0$ ($3p_z$) momentum distribution along the q_x axis.

The study of laser-excited targets opens exciting new avenues. It will be possible to study oriented and aligned targets, and to examine how the remainder of the electron cloud adjusts to one of the electrons being in an excited state. At high laser intensities it should also be possible to do measurements on 'dressed' targets (see for example Joachain *et al.* 1988; Chen 1989).

Acknowledgments

I would like to acknowledge the essential role of I. E. McCarthy in much of the above work. The contributions of P. J. O. Teubner in the establishment of the (e, 2e) technique are gratefully acknowledged. Without the many graduate students, such as S. T. Hood, R. Pascual, P. Storer and Y. Zheng, and the staff of the workshops in the School, very little would have been accomplished. I am also grateful to the ARGC and ARC for financial support of this work.

References

Baker, G. A. Jr, McCarthy, I. E., and Porter, C. E. (1960). *Phys. Rev.* **120**, 254.
Camilloni, R., Giardini-Guidoni, A., Tiribelli, R., and Stefani, G. (1972). *Phys. Rev. Lett.* **29**, 618.
Chen, X. (1989). *Phys. Rev.* A **48**, 1796.
Froese-Fischer, C. (1972). *At. Data* **4**, 301.
Glassgold, A. E., and Ialongo, G. (1968). *Phys. Rev.* **175**, 151.
Hood, S. T., McCarthy, I. E., Teubner, P. J. O., and Weigold, E. (1973*a*). *Phys. Rev.* A **8**, 2494.
Hood, S. T., Weigold, E., McCarthy, I. E., and Teubner, P. J. O. (1973*b*). *Nature Physical Science* **245**, 65.
Joachain, C. J., Franckin, P., Maquet, A., Morton, P., and Veinard, V. (1988). *Phys. Rev. Lett.* **61**, 165.
McCarthy, I. E., Pascual, R., Storer, P., and Weigold, E. (1989). *Phys. Rev.* A **40**, 3041.
McCarthy, I. E., and Weigold, E. (1976). *Phys. Rep.* C **27**, 275.
McCarthy, I. E., and Weigold, E. (1988). *Rep. Prog. Phys.* **51**, 299.
McCarthy, I. E., and Weigold, E. (1990). *Rep. Prog. Phys.* (in press).
Neudatchin, V. G., Novoskol'tseva, G. A., and Smirnov, Yu. F. (1968). *Zh. Eksp. Teor. Fiz.* **55**, 1039 (English translation: *Sov. Phys. JETP* **28**, 540).
Palke, W. E., and Lipscombe, W. N. (1966). *J. Am. Chem. Soc.* **88**, 2384.
Pitzer, R. M. (1967). *J. Chem. Phys.* **46**, 4871.
Smirnov, Yu. F., and Neudatchin, V. G. (1966). *Pis'ma Zh. Eksp. Teor. Fiz.* **3**, 298 (English translation: *JETP Lett. Sov. Phys.* **3**, 192).
Weigold, E. (1990). *Aust. J. Phys.* **43**, 543.
Weigold, E., Hood, S. T., and Teubner, P. J. O. (1973*a*). *Phys. Rev. Lett.* **30**, 475.
Weigold, E., Hood, S. T., McCarthy, I. E., and Teubner, P. J. O. (1973*b*). *Phys. Lett.* A **44**, 531.
Weigold, E., Zheng, Y., and von Niessen, W. (1991). *Chem. Phys.* (in press).
Zheng, Y., McCarthy, I. E., Weigold, E., and Zhang, D. (1990). *Phys. Rev. Lett.* **64**, 1358.

Manuscript received 28 August 1990, accepted 10 January 1991